Journal of Computational Physics **171,** 509–533 (2001)
doi:10.1006/jcph.2001.6788, available online at http://www.idealibrary.com on IDEAL®

Exact Monte Carlo Perturbation Analysis by Forward-Adjoint Coupling in Radiation Transport Calculations

Taro Ueki* and J. Eduard Hoogenboom†

**3-44-1-13 Chiharadai, Ichihara, Chiba 290-0158 Japan; †Interfaculty Reactor Institute, Delft University of Technology, Mekelweg 15, 2629 JB Delft, The Netherlands*
E-mail: taroueki85@hotmail.com; J.E.Hoogenboom@IRI.TUDelft.NL

Received June 22, 2000; revised January 17, 2001

An exact perturbation analysis method in Monte Carlo radiation transport calculations is investigated utilizing the coupling of forward and adjoint simulations. The vehicle chosen for this investigation is correlated-coupling for time-independent neutron or photon transport problems, which has been applied to material perturbation isolated from both the source and detector. By initiating forward and adjoint simulation histories (trajectories) in opposite directions at a position sampled from the interface between the perturbed and unperturbed materials, the correlated-coupling can exclusively construct the physical particle histories traversing the perturbed material. In other words, only those histories that have influence on the variation of the detector response are simulated. There exists no approximation in the sense that all the higher order perturbed terms in the response variation are kept. Moreover, the statistical error is estimated in the same way as in the confidence interval estimation in a standard forward or adjoint calculation. The theoretical basis lies in response decomposition with an enclosure containing both the source and detector. Numerical results are shown for multi-energy group problems.

Key Words: Monte Carlo; radiation transport; coupling; perturbation.

I. INTRODUCTION

In radiation transport calculations, forward Monte Carlo methods solve transport equation [1] by simulating particles born at a physical source based on the probability density functions for various naturally occurring events. The adjoint transport equation is also solved by Monte Carlo methods with an artificially constructed transport mechanism [2, 3] that can be interpreted as backward processes in a sense that simulation particles are born at a physical detector and their scores are collected at the physical source. These standard methods have been practiced for several decades.

0021-9991/01 $35.00

It is sometimes the case that the particle transport from a physical source to a physical detector is decomposed into several naturally occurring or artificially devised transport problems. Two-dimensional spatial surfaces may be placed to couple the forward or adjoint simulations of the decomposed problems. As a straightforward example, forward and adjoint histories (trajectories in state space) are initiated at a physical source and a physical detector, respectively, and the forward and adjoint scores for discretized space–energy–angle cells are tallied at an intermediate surface [4]. As another straightforward example, either forward or adjoint histories are initiated and the discretized scores are tallied at the intermediate surface to create the source distribution for the next stage calculation [5]. On the other hand, forward and adjoint histories can be initiated in exactly opposite directions at the intermediate surface without introducing discretization [6]. This discretization-free coupling method may be called correlated-coupling, since the initially oppositely moving forward and adjoint histories are independent, conditional on their common initial variables. This paper seeks to combine correlated-coupling with the perturbation analysis of a neutron or photon source-detector system.

Physically, the probability of the neutral particle's first entrance to a subdomain does not get affected by a change in the material properties therein. In other words, a physical detector response can be decomposed into a component invariant against, and a component influenced by, material changes in a subdomain. Forward-adjoint coupling methods may be sought to calculate the latter component independently of the former component. This idea is attractive because only the latter component needs to be calculated to evaluate the variation of the detector response, and a radiation detection instrument is generally an independent device to be inserted to measure some properties of a physical system of interest. Moreover, if forward and adjoint simulation histories can be initiated in opposite directions at the interface between perturbed and unperturbed materials, the physical particle histories traversing the perturbed material can be exclusively constructed. This paper specializes in material changes in a subdomain isolated from both physical source and detector. The corresponding Monte Carlo perturbation analysis becomes a very difficult task because only the particle histories that enter and exit the subdomain before reaching the physical detector have real influence on the response variation.

In our previous work [7, 8], various possibilities of correlated-coupling were investigated based on integrals over a spatial surface between a physical source and a physical detector. Similar investigations can also be made in terms of response decomposition with surface integral at an enclosure containing both the physical source and detector. Consequently, the response variation resulting from a material change outside the source-detector enclosure is exactly expressed as the integral over that enclosure of the product of the directional cosine and two flux quantities: The flux in the forward problem for the spatial subdomain with only the unperturbed material and the flux difference between the adjoint problems for the whole spatial domain. Such a surface integral can be computed efficiently by the initial-variable sampling methodologies in the correlated coupling [7, 8]. The resulting computational method has two notable characteristics; first, one Monte Carlo calculation evaluates the variation of a detector response based on an unbiased estimation of the exact integral expression, and second, the statistical error is estimated in the same way as in the confidence interval estimation in a standard forward or adjoint Monte Carlo calculation. In other words, without worrying about which of the first, second, and higher order perturbation treatments is appropriate, one can evaluate response variation by a standard confidence interval estimation using an unbiased sample variance estimator. These characteristics are

advantageous points because standard techniques in Monte Carlo perturbation analysis [9, 10] are generally valid within the framework of finite order perturbation theory, and their error estimation often needs intricate treatments.

II. PROBLEM STATEMENT

A source-detector system for neutron or photon is treated in this paper. We consider material perturbations outside an enclosure containing both the source and detector. We derive integral expressions with the product of forward and adjoint angular fluxes at the enclosure, which can be used to compute quantities difficult to evaluate by a standard forward or adjoint Monte Carlo method.

The volume inside the source-detector enclosure is denoted by V_{SD}, the whole spatial domain by V, and the volume outside the source-detector enclosure $V \setminus V_{SD}$. Figure 1 shows

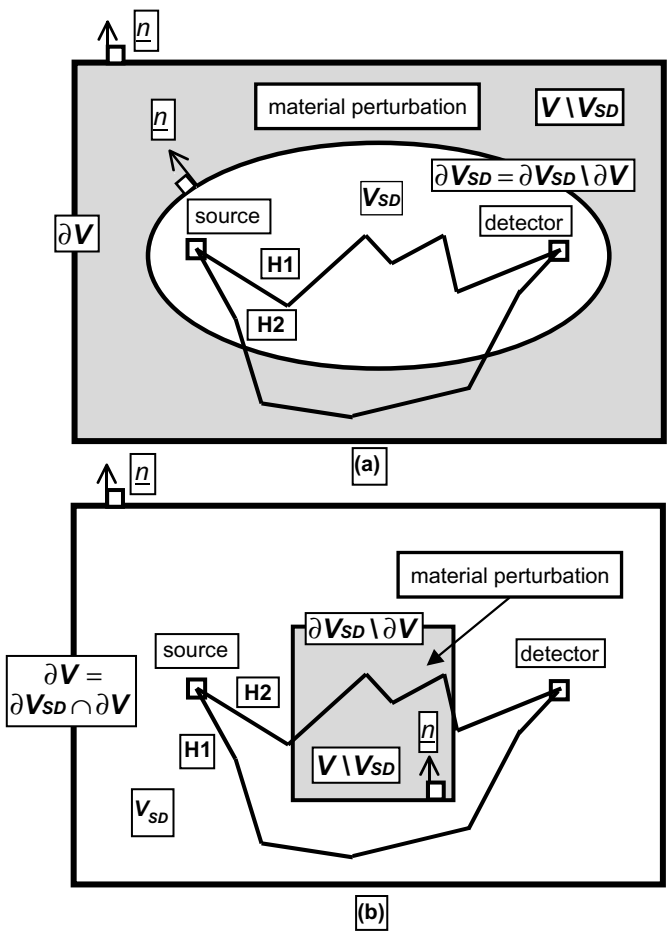

FIG. 1. Source-detector system and material perturbation. (Two perturbation types are shown; the whole spatial domain is denoted by V and its external surface by ∂V; a spatial subdomain containing both the source and detector is denoted by V_{SD} and the surface enclosing that subdomain by ∂V_{SD}; ∂V and ∂V_{SD} have intersection in (b) but do not in (a); material outside V_{SD} is perturbed; particle histories are categorized according to whether they pass the perturbed subdomain or not, H2 or H1.)

examples of the source-detector enclosure. Two problems defined on V are considered:

1. In problem 1, material 1 occupies $V \setminus V_{SD}$ and
2. In problem 2, material 2 occupies $V \setminus V_{SD}$.

Throughout this paper problems 1 and 2 are denoted by P1 and P2, respectively, and the material in V_{SD} is fixed (remains the same for P1 and P2). The source distribution $S(\mathbf{r}, \Omega, E)$ and the detector response function $D(\mathbf{r}, \Omega, E)$ are also fixed. Here, as usual, $\mathbf{r}$ denotes position vector, Ω unit vector of direction of movement, and E energy. We consider the forward and adjoint transport equations for P1 and P2, whose solution express a quantity equivalent to particle flux. The forward equations express naturally occurring particle transport originating from the source. The adjoint equations express artificially devised backward particle transport originating from the detector. They share the same total macroscopic cross section $\Sigma_t(\mathbf{r}, E)$ defined as the mean number of collisions per unit path length travelled. With the interchanged roles of the energies and directions of movements at precollision and at postcollision, the forward and adjoint equations also share differential scattering macroscopic cross section $\Sigma_s(\mathbf{r}, \Omega' \to \Omega, E' \to E)$ whose definition in the forward equation is the mean number of particles with energy in unit interval around E and direction of movement in unit solid angle around Ω per unit path length travelled by the particle with E' and Ω'. (See [1, 11] for details of transport equation.) Also, the following physical observation is important: a change in the material properties in a subdomain affects particle distribution both inside and outside that subdomain, and the solution of the corresponding transport equation is perturbed over the whole spatial domain. Mathematically, this is the consequence of a continuity condition of transport equation.

III. THEORETICAL DEVELOPMENT

The purpose of this section is to obtain the exact surface integral expression of the response variation from P1 to P2. The forward transport equation for P1 is ([1, 11]):

$$\begin{aligned}
&\Omega \cdot \nabla \Psi_1(\mathbf{r}, \Omega, E) + \Sigma_t(\mathbf{r}, E)\Psi_1(\mathbf{r}, \Omega, E) \\
&\quad = \int_0^{E_0} \int_{4\pi} \Sigma_s(\mathbf{r}, \Omega' \to \Omega, E' \to E)\Psi_1(\mathbf{r}, \Omega', E')\, d\Omega' dE' \\
&\qquad + S(\mathbf{r}, \Omega, E) \quad \text{for } \mathbf{r} \in V_{SD}, \qquad (1) \\
&\Omega \cdot \nabla \Psi_1(\mathbf{r}, \Omega, E) + \Sigma_{1,t}(\mathbf{r}, \Omega, E)\Psi_1(\mathbf{r}, \Omega, E) \\
&\quad = \int_0^{E_0} \int_{4\pi} \Sigma_{1,s}(\mathbf{r}, \Omega' \to \Omega, E' \to E)\Psi_1(\mathbf{r}, \Omega', E')\, d\Omega' dE' \quad \text{for } \mathbf{r} \in V \setminus V_{SD}, \qquad (2) \\
&\Psi_1(\mathbf{r}, \Omega, E) = 0 \quad \text{for } \mathbf{r} \in \partial V \text{ and } \Omega \cdot \mathbf{n} < 0, \qquad (3)
\end{aligned}$$

with a continuity condition,

$$\lim_{\epsilon \downarrow 0} \Psi_1(\mathbf{r} - \epsilon\Omega, \Omega, E) = \lim_{\epsilon \downarrow 0} \Psi_1(\mathbf{r} + \epsilon\Omega, \Omega, E) \quad \text{for } \mathbf{r} \in \partial V_{SD} \setminus \partial V,$$

where the macroscopic cross sections in Eq. (1) correspond to a fixed (never perturbed) material in V_{SD}; the subscript 1 of the macroscopic cross sections in Eq. (2) implies that

$V\backslash V_{SD}$ is occupied by material 1; the subscript 1 in the forward angular flux stands for the solution corresponding to such material distribution; 4π denotes the unit spherical surface with its center at the origin; and E_0 is the maximum energy allowed in the physical problem under consideration. Throughout this paper, "∂" denotes the surface of a volume and "\" the relative complement of a set (the difference of sets); $r \in \partial V_{SD}\backslash\partial V$ implies that r belongs to ∂V_{SD} but does not belong to ∂V. Equations (1) and (2) may be written as

$$\Omega \cdot \nabla\Psi_1(r, \Omega, E) + \Sigma_{1,t}(r, \Omega, E)\Psi_1(r, \Omega, E)$$
$$= \int_0^{E_0} \int_{4\pi} \Sigma_{1,s}(r, \Omega' \to \Omega, E' \to E)\Psi_1(r, \Omega', E')\, d\Omega'\, dE' + S(r, \Omega, E) \quad \text{for } r \in V,$$
$$\Sigma_{1,t}(r, \Omega, E) = \Sigma_t(r, E) \quad \text{for } r \in V_{SD},$$
$$\Sigma_{1,s}(r, \Omega' \to \Omega, E' \to E) = \Sigma_s(r, \Omega' \to \Omega, E' \to E) \quad \text{for } r \in V_{SD},$$
$$S(r, \Omega, E) = 0 \quad \text{for } r \in V\backslash V_{SD}.$$

The above equations emphasize that the material in V_{SD} is fixed (remains unperturbed), and the region outside V_{SD} is occupied by any material designated as 1, while Eqs. (1) and (2) emphasize the explicit form in V_{SD} and in $V\backslash V_{SD}$, respectively, taken by the forward transport equation for P1. This paper follows the style of Eqs. (1) and (2). The unnumbered continuity condition clarifies that there is no singular source such as a point or surface source at $\partial V_{SD}\backslash\partial V$; the source is strictly contained inside V_{SD}. The adjoint transport equation for P2 is ([11])

$$-\Omega \cdot \nabla\Psi_2^*(r, \Omega, E) + \Sigma_t(r, E)\Psi_2^*(r, \Omega, E)$$
$$= \int_0^{E_0} \int_{4\pi} \Sigma_s(r, \Omega \to \Omega', E \to E')\Psi_2^*(r, \Omega', E')\, d\Omega' dE'$$
$$+ D(r, \Omega, E) \quad \text{for } r \in V_{SD}, \tag{4}$$
$$-\Omega \cdot \nabla\Psi_2^*(r, \Omega, E) + \Sigma_{2,t}(r, \Omega, E)\Psi_2^*(r, \Omega, E)$$
$$= \int_0^{E_0} \int_{4\pi} \Sigma_{2,s}(r, \Omega \to \Omega', E \to E')\Psi_2^*(r, \Omega', E')\, d\Omega' dE' \quad \text{for } r \in V\backslash V_{SD}, \tag{5}$$
$$\Psi_2^*(r, \Omega, E) = 0 \quad \text{for } r \in \partial V \text{ and } \Omega \cdot n > 0, \tag{6}$$

with a continuity condition,

$$\lim_{\epsilon \downarrow 0} \Psi_2^*(r - \epsilon\Omega, \Omega, E) = \lim_{\epsilon \downarrow 0} \Psi_2^*(r + \epsilon\Omega, \Omega, E) \quad \text{for } r \in \partial V_{SD}\backslash\partial V,$$

where the macroscopic cross sections in Eq. (4) are the same as those in Eq. (1); the subscript 2 of the macroscopic cross sections in Eq. (5) implies that V_{SD} is occupied by any material designated as 2; and the subscript 2 in the adjoint angular flux stands for the solution corresponding to such material distribution. The unnumbered continuity condition clarifies that there is no singular detector such as a point or surface detector at $\partial V_{SD}\backslash\partial V$; the detector is strictly contained inside V_{SD}.

We multiply Eq. (1) by Ψ_2^* and Eq. (4) by Ψ_1, subtract the latter from the former, integrate over V_{SD}, direction of movement and energy. The terms with the total macroscopic cross section cancel out. The terms with the differential scattering macroscopic cross section

cancel out by interchanging the integration variables Ω, E and Ω', E' in one of these terms. Then, converting the remaining volume integral (dV) in the left-hand side to the surface integral (dA) by the divergence theorem, one obtains

$$\begin{aligned}\int_{\partial V_{SD}\backslash\partial V}\int_{4\pi}\int_0^{E_0} n\cdot\Omega\Psi_1(r,\Omega,E)\Psi_2^*(r,\Omega,E)\,dE\,d\Omega\,dA \\ = \int_{V_{SD}}\int_{4\pi}\int_0^{E_0} S(r,\Omega,E)\Psi_2^*(r,\Omega,E)\,dE\,d\Omega\,dV \\ - \int_{V_{SD}}\int_{4\pi}\int_0^{E_0} D(r,\Omega,E)\Psi_1(r,\Omega,E)\,dE\,d\Omega\,dV, \qquad (7)\end{aligned}$$

where in the left-hand side the surface integration domain is intended to cover both (a) and (b) in Fig. 1 with the consideration of the external boundary conditions (3) and (6) for the latter. The second term in the right-hand side of Eq. (7) is the physical detector response of P1 [11, 12]:

$$R_1 = \int_{V_{SD}}\int_{4\pi}\int_0^{E_0} D(r,\Omega,E)\Psi_1(r,\Omega,E)\,dE\,d\Omega\,dV. \qquad (8)$$

The first term in the right-hand side of Eq. (7) is the physical detector response of P2 [11, 12]:

$$R_2 = \int_{V_{SD}}\int_{4\pi}\int_0^{E_0} S(r,\Omega,E)\Psi_2^*(r,\Omega,E)\,dE\,d\Omega\,dV. \qquad (9)$$

Therefore, Eq. (7) is rewritten as

$$R_2 - R_1 = \int_{\partial V_{SD}\backslash\partial V}\int_{4\pi}\int_0^{E_0} n\cdot\Omega\Psi_1(r,\Omega,E)\Psi_2^*(r,\Omega,E)\,dE\,d\Omega\,dA. \qquad (10)$$

The roles of the forward and the adjoint equations can be interchanged. The adjoint transport equation for P1 is ([1, 11])

$$\begin{aligned}-\Omega\cdot\nabla\Psi_1^*(r,\Omega,E) + \Sigma_t(r,E)\Psi_1^*(r,\Omega,E) \\ = \int_0^{E_0}\int_{4\pi}\Sigma_s(r,\Omega\to\Omega',E\to E')\Psi_1^*(r,\Omega',E')\,d\Omega'\,dE' \\ + D(r,\Omega,E) \quad \text{for } r\in V_{SD}, \qquad (11)\\ -\Omega\cdot\nabla\Psi_1^*(r,\Omega,E) + \Sigma_{1,t}(r,\Omega,E)\Psi_1^*(r,\Omega,E) \\ = \int_0^{E_0}\int_{4\pi}\Sigma_{1,s}(r,\Omega\to\Omega',E\to E')\Psi_1^*(r,\Omega',E')\,d\Omega'\,dE' \quad \text{for } r\in V\backslash V_{SD}, \qquad (12)\\ \Psi_1^*(r,\Omega,E) = 0 \quad \text{for } r\in\partial V \text{ and } \Omega\cdot n>0, \qquad (13)\end{aligned}$$

with a continuity condition,

$$\lim_{\epsilon\downarrow 0}\Psi_1^*(r-\epsilon\Omega,\Omega,E) = \lim_{\epsilon\downarrow 0}\Psi_1^*(r+\epsilon\Omega,\Omega,E) \quad \text{for } r\in\partial V_{SD}\backslash\partial V.$$

The forward transport equation for P2 is ([1, 11])

$$\Omega \cdot \nabla \Psi_2(r, \Omega, E) + \Sigma_t(r, E)\Psi_2(r, \Omega, E)$$
$$= \int_0^{E_0} \int_{4\pi} \Sigma_s(r, \Omega' \to \Omega, E' \to E)\Psi_2(r, \Omega', E')\, d\Omega'\, dE'$$
$$+ S(r, \Omega, E) \quad \text{for } r \in V_{SD}, \tag{14}$$

$$\Omega \cdot \nabla \Psi_2(r, \Omega, E) + \Sigma_{2,t}(r, \Omega, E)\Psi_2(r, \Omega, E)$$
$$= \int_0^{E_0} \int_{4\pi} \Sigma_{2,s}(r, \Omega' \to \Omega, E' \to E)\Psi_2(r, \Omega', E')\, d\Omega'\, dE' \quad \text{for } r \in V \backslash V_{SD}, \tag{15}$$

$$\Psi_2(r, \Omega, E) = 0 \quad \text{for } r \in \partial V \text{ and } \Omega \cdot n < 0, \tag{16}$$

with a continuity condition,

$$\lim_{\epsilon \downarrow 0} \Psi_2(r - \epsilon\Omega, \Omega, E) = \lim_{\epsilon \downarrow 0} \Psi_2(r + \epsilon\Omega, \Omega, E) \quad \text{for } r \in \partial V_{SD} \backslash \partial V.$$

By taking the steps similar to those leading to Eq. (7), Eqs. (11), (13), (14), and (16) yield

$$\int_{\partial V_{SD} \backslash \partial V} \int_{4\pi} \int_0^{E_0} n \cdot \Omega \Psi_2(r, \Omega, E)\Psi_1^*(r, \Omega, E)\, dE\, d\Omega\, dA$$
$$= \int_{V_{SD}} \int_{4\pi} \int_0^{E_0} S(r, \Omega, E)\Psi_1^*(r, \Omega, E)\, dE\, d\Omega\, dV$$
$$- \int_{V_{SD}} \int_{4\pi} \int_0^{E_0} D(r, \Omega, E)\Psi_2(r, \Omega, E)\, dE\, d\Omega\, dV. \tag{17}$$

In addition to Eqs. (8) and (9), R_1 and R_2 can also be expressed as

$$R_1 = \int_{V_{SD}} \int_{4\pi} \int_0^{E_0} S(r, \Omega, E)\Psi_1^*(r, \Omega, E)\, dE\, d\Omega\, dV, \tag{18}$$

and

$$R_2 = \int_{V_{SD}} \int_{4\pi} \int_0^{E_0} D(r, \Omega, E)\Psi_2(r, \Omega, E)\, dE\, d\Omega\, dV \tag{19}$$

by references [11, 12]. Eq. (17) is rewritten as

$$R_1 - R_2 = \int_{\partial V_{SD} \backslash \partial V} \int_{4\pi} \int_0^{E_0} n \cdot \Omega \Psi_2(r, \Omega, E)\Psi_1^*(r, \Omega, E)\, dE\, d\Omega\, dA. \tag{20}$$

Since Eqs. (11)–(13) and (14)–(16) have simply interchanged the roles of the forward and adjoint problems in Eqs. (1)–(3) and (4)–(6), Eq. (20) can be also obtained by interchanging the subscripts "1" and "2" in Eq. (10).

We consider a special problem wherein a black absorber occupies $V \backslash V_{SD}$. Here, the black absorber has the total macroscopic cross section of infinite magnitude and the differential scatterring macroscopic cross section of a zero value. PB is used to denote such a special problem. In previous work, the so-called black absorber technique (perturbation) was utilized [4, 7]. The difference between the previous work and the work in this paper resides

in the setup of a spatial surface at which the bilinear integral of forward and adjoint fluxes is defined to be calculated. In the former work, the spatial surface encloses either source or detector, while in the latter work it encloses both source and detector. Now, we turn to the forward and adjoint transport equation for PB:

$$\begin{aligned}
&\Omega \cdot \nabla \Psi_B(\boldsymbol{r}, \Omega, E) + \Sigma_t(\boldsymbol{r}, E)\Psi_B(\boldsymbol{r}, \Omega, E) \\
&\quad = \int_0^{E_0} \int_{4\pi} \Sigma_s(\boldsymbol{r}, \Omega' \to \Omega, E' \to E)\Psi_B(\boldsymbol{r}, \Omega', E')\, d\Omega'\, dE' \\
&\qquad + S(\boldsymbol{r}, \Omega, E) \quad \text{for } \boldsymbol{r} \in V_{SD}, \qquad (21) \\
&\Psi_B(\boldsymbol{r}, \Omega, E) = 0 \quad \text{for } \boldsymbol{r} \in \partial V_{SD} \text{ and } \Omega \cdot \boldsymbol{n} < 0, \qquad (22)
\end{aligned}$$

and

$$\begin{aligned}
&-\Omega \cdot \nabla \Psi_B^*(\boldsymbol{r}, \Omega, E) + \Sigma_t(\boldsymbol{r}, E)\Psi_B^*(\boldsymbol{r}, \Omega, E) \\
&\quad = \int_0^{E_0} \int_{4\pi} \Sigma_s(\boldsymbol{r}, \Omega \to \Omega', E \to E')\Psi_B^*(\boldsymbol{r}, \Omega', E')\, d\Omega'\, dE' \\
&\qquad + D(\boldsymbol{r}, \Omega, E) \quad \text{for } \boldsymbol{r} \in V_{SD}, \qquad (23) \\
&\Psi_B^*(\boldsymbol{r}, \Omega, E) = 0 \quad \text{for } \boldsymbol{r} \in \partial V_{SD} \text{ and } \Omega \cdot \boldsymbol{n} > 0. \qquad (24)
\end{aligned}$$

The physical detector response of PB is expressed as ([11, 12])

$$\begin{aligned}
R_B &= \int_{V_{SD}} \int_{4\pi} \int_0^{E_0} S(\boldsymbol{r}, \Omega, E)\Psi_B^*(\boldsymbol{r}, \Omega, E)\, dE\, d\Omega\, dV \\
&= \int_{V_{SD}} \int_{4\pi} \int_0^{E_0} D(\boldsymbol{r}, \Omega, E)\Psi_B(\boldsymbol{r}, \Omega, E)\, dE\, d\Omega\, dV. \qquad (25)
\end{aligned}$$

We make material 1 purely absorbing ($\Sigma_{1,s} = 0$) and let its total macroscopic cross section tend to infinity ($\Sigma_{1,t} \to \infty$). The uncollided escape probability of the forward and adjoint simulation particles from the purely absorbing material in $V \backslash V_{SD}$, then, monotonically decreases to zero. This implies that Ψ_1 and Ψ_1^* monotonically decrease to Ψ_B and Ψ_B^*:

$$\Psi_1 \downarrow \Psi_B \quad \text{and} \quad \Psi_1^* \downarrow \Psi_B^* \quad \text{as } \Sigma_{1,t} \to \infty \text{ with } \Sigma_{1,s} = 0.$$

Thus, when the limit operation $\Sigma_{1,t} \to \infty$ with $\Sigma_{1,s} = 0$ is applied to Eqs. (8), (10), (18), and (20), Ψ_1 and Ψ_1^* are bounded by integrable functions that are the particular versions of Ψ_1 and Ψ_1^* resulting from setting $\Sigma_{1,s} = 0$ and $\Sigma_{1,t}$ fixed-finite. The dominated convergence theorem [13] allows one to interchange the order of the integral and limit in Eqs. (8) and (18) as

$$\begin{aligned}
\lim_{\Sigma_{1,t}\to\infty, \Sigma_{1,s}=0} R_1 &= \lim_{\Sigma_{1,t}\to\infty, \Sigma_{1,s}=0} \int_{V_{SD}} \int_{4\pi} \int_0^{E_0} D(\boldsymbol{r}, \Omega, E)\Psi_1(\boldsymbol{r}, \Omega, E)\, dE\, d\Omega\, dV \\
&= \int_{V_{SD}} \int_{4\pi} \int_0^{E_0} D(\boldsymbol{r}, \Omega, E) \lim_{\Sigma_{1,t}\to\infty, \Sigma_{1,s}=0} \Psi_1(\boldsymbol{r}, \Omega, E)\, dE\, d\Omega\, dV \\
&= \int_{V_{SD}} \int_{4\pi} \int_0^{E_0} D(\boldsymbol{r}, \Omega, E)\Psi_B(\boldsymbol{r}, \Omega, E)\, dE\, d\Omega\, dV \\
&= R_B,
\end{aligned}$$

and

$$\begin{aligned}\lim_{\Sigma_{1,t}\to\infty,\Sigma_{1,s}=0} R_1 &= \lim_{\Sigma_{1,t}\to\infty,\Sigma_{1,s}=0} \int_{V_{SD}}\int_{4\pi}\int_0^{E_0} S(r,\Omega,E)\Psi_1^*(r,\Omega,E)\,dE\,d\Omega\,dV \\ &= \int_{V_{SD}}\int_{4\pi}\int_0^{E_0} S(r,\Omega,E) \lim_{\Sigma_{1,t}\to\infty,\Sigma_{1,s}=0} \Psi_1^*(r,\Omega,E)\,dE\,d\Omega\,dV \\ &= \int_{V_{SD}}\int_{4\pi}\int_0^{E_0} S(r,\Omega,E)\Psi_B^*(r,\Omega,E)\,dE\,d\Omega\,dV \\ &= R_B,\end{aligned}$$

where Eq. (25) was used for the equalities before R_B. Similarly, the dominated convergence theorem is applied to the right-hand side of Eqs. (10) and (20) as

$$\begin{aligned}&\lim_{\Sigma_{1,t}\to\infty,\Sigma_{1,s}=0} \int_{\partial V_{SD}\setminus\partial V}\int_{4\pi}\int_0^{E_0} n\cdot\Omega\Psi_1(r,\Omega,E)\Psi_2^*(r,\Omega,E)\,dE\,d\Omega\,dA. \\ &= \int_{\partial V_{SD}\setminus\partial V}\int_{4\pi}\int_0^{E_0} n\cdot\Omega \lim_{\Sigma_{1,t}\to\infty,\Sigma_{1,s}=0} \Psi_1(r,\Omega,E)\Psi_2^*(r,\Omega,E)\,dE\,d\Omega\,dA \\ &= \int_{\partial V_{SD}\setminus\partial V}\int_{4\pi}\int_0^{E_0} n\cdot\Omega\Psi_B(r,\Omega,E)\Psi_2^*(r,\Omega,E)\,dE\,d\Omega\,dA,\end{aligned}$$

and

$$\begin{aligned}&\lim_{\Sigma_{1,t}\to\infty,\Sigma_{1,s}=0} \int_{\partial V_{SD}\setminus\partial V}\int_{4\pi}\int_0^{E_0} n\cdot\Omega\Psi_2(r,\Omega,E)\Psi_1^*(r,\Omega,E)\,dE\,d\Omega\,dA \\ &= \int_{\partial V_{SD}\setminus\partial V}\int_{4\pi}\int_0^{E_0} n\cdot\Omega\Psi_2(r,\Omega,E) \lim_{\Sigma_{1,t}\to\infty,\Sigma_{1,s}=0} \Psi_1^*(r,\Omega,E)\,dE\,d\Omega\,dA \\ &= \int_{\partial V_{SD}\setminus\partial V}\int_{4\pi}\int_0^{E_0} n\cdot\Omega\Psi_2(r,\Omega,E)\Psi_B^*(r,\Omega,E)\,dE\,d\Omega\,dA.\end{aligned}$$

Hence, by taking into account the fact that R_2 is constant with respect to $\Sigma_{1,t}$ and $\Sigma_{1,s}$, Eqs. (10) and (20) with $\Sigma_{1,t}\to\infty$ and $\Sigma_{1,s}=0$ yield

$$R_2 = R_B + \int_{\partial V_{SD}\setminus\partial V}\int_{n\cdot\Omega>0}\int_0^{E_0} n\cdot\Omega\Psi_B(r,\Omega,E)\Psi_2^*(r,\Omega,E)\,dE\,d\Omega\,dA, \tag{26}$$

and

$$\begin{aligned}R_2 &= R_B - \int_{\partial V_{SD}\setminus\partial V}\int_{n\cdot\Omega<0}\int_0^{E_0} n\cdot\Omega\Psi_2(r,\Omega,E)\Psi_B^*(r,\Omega,E)\,dE\,d\Omega\,dA \\ &= R_B + \int_{\partial V_{SD}\setminus\partial V}\int_{n\cdot\Omega<0}\int_0^{E_0} |n\cdot\Omega|\Psi_2(r,\Omega,E)\Psi_B^*(r,\Omega,E)\,dE\,d\Omega\,dA. \end{aligned}\tag{27}$$

By interchanging the forward and adjoint roles of P1 and P2, one obtains

$$R_1 = R_B + \int_{\partial V_{SD}\setminus\partial V}\int_{n\cdot\Omega>0}\int_0^{E_0} n\cdot\Omega\Psi_B(r,\Omega,E)\Psi_1^*(r,\Omega,E)dEd\Omega dA, \tag{28}$$

and

$$R_1 = R_B - \int_{\partial V_{SD}\setminus\partial V}\int_{n\cdot\Omega<0}\int_0^{E_0} n\cdot\Omega\Psi_1(r,\Omega,E)\Psi_B^*(r,\Omega,E)\,dE\,d\Omega\,dA$$
$$= R_B + \int_{\partial V_{SD}\setminus\partial V}\int_{n\cdot\Omega<0}\int_0^{E_0} |n\cdot\Omega|\Psi_1(r,\Omega,E)\Psi_B^*(r,\Omega,E)\,dE\,d\Omega\,dA. \quad (29)$$

Equations (26)–(29) are mathematical statements of response decomposition: *a detector response is decomposed into the components resulting from particle histories either confined inside a source-detector enclosure or crossing and recrossing the same enclosure.* The first term in Eqs. (26)–(29) is the response resulting from the physical particle histories designated as "H1" in Fig. 1 and is invariant with respect to material changes outside the source-detector enclosure. The second term in the same equations is the response resulting from the physical particle histories designated as "H2" in Figure 1 and is influened by the foregoing changes. Equations. (26) and (28) yield

$$R_1 - R_2 = \int_{\partial V_{SD}\setminus\partial V}\int_{n\cdot\Omega>0}\int_0^{E_0} n\cdot\Omega\Psi_B(r,\Omega,E)$$
$$\times[\Psi_1^*(r,\Omega,E) - \Psi_2^*(r,\Omega,E)]\,dE\,d\Omega\,dA, \quad (30)$$

and Eqs. (27) and (29) yield

$$R_1 - R_2 = \int_{\partial V_{SD}\setminus\partial V}\int_{n\cdot\Omega<0}\int_0^{E_0} |n\cdot\Omega|$$
$$\times[\Psi_1(r,\Omega,E) - \Psi_2(r,\Omega,E)]\Psi_B^*(r,\Omega,E)\,dE\,d\Omega\,dA. \quad (31)$$

Equations (30) and (31) are the exact expressions of the response variation from P1 to P2.

There exists previous work that is physically different from, but resembles in appearance, the work in this paper. Hoffman *et al.* studied response at a detector placed inside a perturbing material [14]. This is obviously different from the physical problem analyzed in this section. However, since the response can be expressed by a surface integral at the enclosure encompassing the perturbing material, mathematical expressions similar in appearance to Eqs. (30) and (31) appeared in the work of Hoffman *et al.* On the other hand, Sánchez has shown that the convolution of Green's functions can systematically analyze a pair of problems whose material distributions coincide in their common subdomain [15]. When the domain of one problem is contained in the domain of the other problem, the paired problems play the same role as P1 and PB or P2 and PB. Therefore, despite the apparent difference in methodologies employed, the perturbation analysis in this section is closely related to the Green's function method in the work of Sánchez.

We compute Eq. (30) following the procedures in correlated coupling [7, 8]. To do this, an arbitrary nonzero space–energy distribution function is introduced:

$$\int_{\partial V_{SD}\setminus\partial V}\int_0^{E_0} f(r,E)\,dE\,dA = 1,\ f(r,E) > 0.$$

One may utilize the discretized energy group structure in a nuclear cross section library; $f(r,E) = (1/G)\sum_{g=1}^{G} f_g(r,E)$ where $\int_{\partial V_{SD}\setminus\partial V}\int_{E_g}^{E_{g-1}} f_g(r,E)\,dE\,dA = 1$, $f_g(r,E) = 0$

for E outside (E_g, E_{g-1}) and $0 = E_G < \cdots < E_0$. Eq. (30) is then rewritten as

$$R_1 - R_2 = \int_{\partial V_{SD}\setminus\partial V} \int_{\mathbf{n}\cdot\Omega>0} \int_0^{E_0} \frac{\pi}{f(\mathbf{r}, E)} \Psi_B(\mathbf{r}, \Omega, E)[\Psi_1^*(\mathbf{r}, \Omega, E) - \Psi_2^*(\mathbf{r}, \Omega, E)] \frac{f(\mathbf{r}, E)\mathbf{n}\cdot\Omega}{\pi} dE\, d\Omega\, dA. \tag{32}$$

Here, we consider $f(\mathbf{r}, E)\mathbf{n}\cdot\Omega/\pi$ the probability density function of initial variables because $\int_{\partial V_{SD}\setminus\partial V} \int_{\mathbf{n}\cdot\Omega>0} \int_0^{E_0} [f(\mathbf{r}, E)\mathbf{n}\cdot\Omega/\pi]\, dE\, d\Omega\, dA = 1$. The sampling from $f(\mathbf{r}, E)\mathbf{n}\cdot\Omega/\pi$ then corresponds to the initial (source) variable sampling in a standard forward or adjoint Monte Carlo calculation, and $\pi/f(\mathbf{r}, E)$ becomes an initial position-energy dependent multiplier. Conditional on the sampled initial variables $(\mathbf{r}, \Omega, E) = (\mathbf{r}_I, \Omega_I, E_I)$, the formally adjoint problems of Eqs. (21) and (22), Eqs. (11)–(13), and Eqs. (4)–(6) are constructed with the unit monoenergetic and monodirectional point source or detector for $(\mathbf{r}_I, \Omega_I, E_I)$ in order to calculate $\Psi_B(\mathbf{r}_I, \Omega_I, E_I)$, $\Psi_1^*(\mathbf{r}_I, \Omega_I, E_I)$, and $\Psi_2^*(\mathbf{r}_I, \Omega_I, E_I)$, respectively, by independent Monte Carlo simulations. See Appendix A about these formally adjoint problems. The product of the score for $\Psi_B(\mathbf{r}_I, \Omega_I, E_I)$ and the score difference for $\Psi_1^*(\mathbf{r}_I, \Omega_I, E_I)$ and $\Psi_2^*(\mathbf{r}_I, \Omega_I, E_I)$ multipled by $\pi/f(\mathbf{r}_I, E_I)$ is a statistical entity. Conditional independence [16] ensures that the conditional expectation assuming the sampled initial variables $(\mathbf{r}_I, \Omega_I, E_I)$ is $[\pi/f(\mathbf{r}_I, E_I)]\Psi_B(\mathbf{r}_I, \Omega_I, E_I)\,[\Psi_1^*(\mathbf{r}_I, \Omega_I, E_I) - \Psi_2^*(\mathbf{r}_I, \Omega_I, E_I)]$. This quantity integrated with the probability density function $f(\mathbf{r}_I, E_I)\mathbf{n}\cdot\Omega_I/\pi$ of the initial variables $(\mathbf{r}_I, \Omega_I, E_I)$ becomes the expected value of the proposed computational procedures by the theory of conditional expectation [17]. This yields unbiasedness. See Fig. 2 for the initial movements corresponding to $(\mathbf{r}_I, \Omega_I, E_I)$. Since adjoint simulation particles move in the direction opposite to Ω, the forward and adjoint simulation particles are initiated in exactly opposite directions at $\mathbf{r}_I$. Moreover, the particle's histories

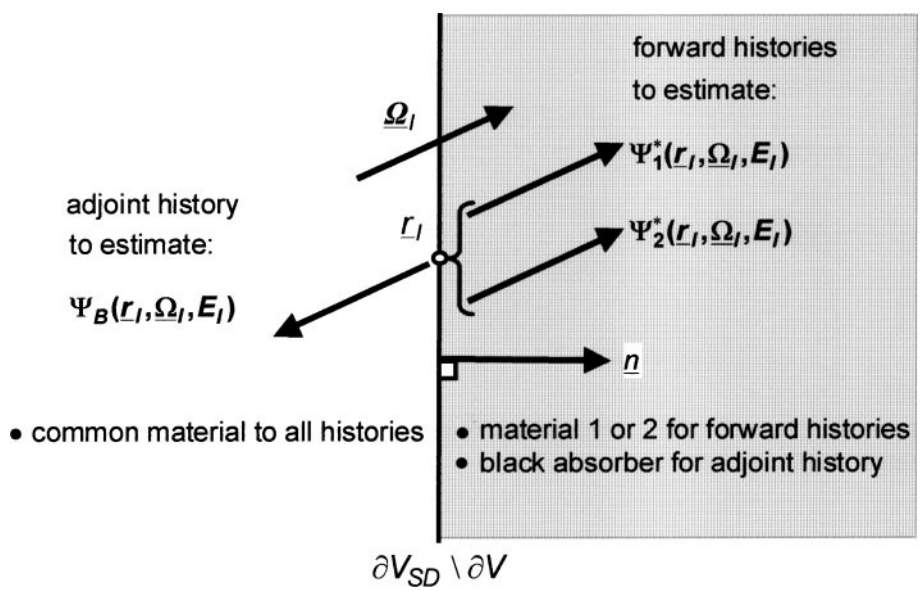

FIG. 2. Initial movements of forward and adjoint histories to compute Eq. (30) (sampled initial variables are position $\mathbf{r}_1$, energy E_1 and direction Ω).

are initiated at the boundary between fixed and variable materials (perturbed and unperturbed subdomains). These two aspects correspond to exclusively constructing the physical particle history traversing perturbed material. The development in this section shows that the calculation of a response variation is a new application area to correlated coupling of forward and adjoint histories.

There are several notable characteristics in the proposed computational scheme. First, the procedure of taking the difference between the results from two independent Monte Carlo calculations after all the histories are completed is avoided with no approximation in a sense that all the higher order perturbed terms are kept. Recall that the score difference for $\Psi_1^*(\mathbf{r}_I, \Omega_I, E_I)$ and $\Psi_2^*(\mathbf{r}_I, \Omega_I, E_I)$ is simply calculated at each sampling of $(\mathbf{r}_I, \Omega_I, E_I)$. Second, the statistical error is estimated in the same way as in the confidence interval estimation in a standard forward or adjoint simulation because upon sampling $(\mathbf{r}_I, \Omega_I, E_I)$ from $f(\mathbf{r}, E)\mathbf{n}\cdot\Omega/\pi$, a statistical entity becomes

$$\begin{aligned}&\frac{\pi}{f(\mathbf{r}_I, E_I)}[\text{adjoint Monte Carlo score for } \Psi_B(\mathbf{r}_I, \Omega_I, E_I)]\\ &\quad\times\{[\text{forward Monte Carlo score for } \Psi_1^*(\mathbf{r}_I, \Omega_I, E_I)]\\ &\qquad-[\text{forward Monte Carlo score for } \Psi_2^*(\mathbf{r}_I, \Omega_I, E_I)]\}.\end{aligned}\tag{33}$$

Since $(\mathbf{r}_I, \Omega_I, E_I)$ are sampled independently, variance estimation by the sample variance formula is unbiased. Those two characteristics can be advantageous points over standard techniques in Monte Carlo perturbation analysis [9, 10].

Equation (31) is also rewritten as

$$\begin{aligned}R_1-R_2=\int_{\partial V_{SD}\setminus\partial V}\int_{\mathbf{n}:\Omega<0}\int_0^{E_0}\frac{\pi}{f(\mathbf{r},E)}[\Psi_1(\mathbf{r},\Omega,E)\\ -\Psi_2(\mathbf{r},\Omega,E)]\Psi_B^*(\mathbf{r},\Omega,E)\frac{f(\mathbf{r},E)|\mathbf{n}\cdot\Omega|}{\pi}\,dE\,d\Omega\,dA.\end{aligned}\tag{34}$$

All the foregoing arguments after Eq. (32) can be made with the interchanged roles of forward and adjoint problems. They are straightforward and obvious, and their presentation is omitted.

The analysis in this section remains valid as far as the following conditions are satisfied: there exists a path connecting a physical source and a physical detector only through fixed material (unperturbed subdomain), and both the source and detector are isolated from variable material (perturbed subdomain). One can then consider a source-detector enclosure whose inside exclusively contains the unperturbed subdomain. However, for problems wherein any source-detector enclosure always contains part of the perturbed subdomain, the analysis leading to Eqs. (26)–(29) becomes invalid. Such problems are related to the problem treated by the adjoint difference method by Hoffman *et al.* [14]. See Appendix B for details.

IV. NUMERICAL RESULTS

Numerical results are shown for multi-energy group problems with the group macroscopic cross sections derived in an approximate way [11]. One of the reasons for this is

that continuous energy adjoint Monte Carlo is not available in full generality [18]. The other reason is that multi-energy group problems serve the purpose of numerically showing the correctness of the proposed correlated coupling procedures. All calculations are done by the MCNP code [19] for neutral radiation particle transport with a new correlated coupling option incorporated by the authors of this paper. Results from the correlated coupling are compared with those from taking the difference between two independent standard forward calculations after the completion of all the histories. Here, the word "standard" is intended to imply that a simulation particle is born at a physical source and its score is tallied at a physical detector. The reason for the foregoing comparison is that correlated coupling unbiasedly computes the exact expression of response variation in Eqs. (30) and (31) with the statistical error unbiasedly estimated in the same way as standard forward calculations. The comparison should be made with a method with no approximation and an unbiased sample variance estimation. Implicit particle capture with weight multiplication is used. Parameters for Russian roulette are set uniformly over all energy and spatial domains and are the same for the two independent standard forward calculations and the forward and adjoint calculations in the correlated coupling. The density function $f(x, E)$ for initial-variable sampling is taken to be uniform over space and energy groups.

Batch-average product processing [7], the calculation of the three batch-averages for the scores in Eq. (33), is employed. This is because when the product of two stochastic quantities is processed as one statistical entity, its statistical porperty improves in a hybrid fashion as the statistical properties of both the quantities improve, and this effect often overcomes the increase of computational time. The advantage of batch-average product processing was numerically demonstrated in [7]. Upon sampling initial-variables based on Eq. (32), the forward flux in Eq. (30) is calculated by a batch of adjoint simulations. When all of the simulations yield a zero score, zero is recorded as a statistical entity, the succeeding forward simulations for the two adjoint fluxes in Eq. (30) are skipped and the next initial-variables are sampled. When some of the preceding adjoint simulations yield nonzero scores, the succeeding two batches of forward simulations are implemented, and Eq. (33) with the three batch-averaged scores is recorded as a statistical entity. The number of histories per batch is taken to be larger for the succeeding simulations than for the preceding simulation following numerical analysis in [7]. In the calculation of Eq. (31) with the initial-variable sampling based on Eq. (34), the role of forward and adjoint simulations are interchanged. The adjoint flux in Eq. (31) is calculated by a batch of forward simulations. When all of the simulations yield a zero score, zero is recorded as a statistical entity, the succeeding adjoint simulations for the two forward fluxes in Eq. (31) are skipped and the next initial-variables are sampled. When some of the preceding forward simulations yield nonzero scores, the succeeding two batches of adjoint simulations are implemented and the three batch-averaged scores are processed as in Eq. (33) with the interchaned roles of the forward and adjoint simulations and fluxes.

Table I shows three energy group macroscopic cross sections for fictitious materials. The values of these macroscopic cross sections are intended to explore a characteristic feature of the proposed procedures. Figure 3 shows the arrangement of a source, a detector, and perturbed spatial subdomains, cubes 1 and 2. Material inside either cube 1 or 2 is perturbed. The material in the unperturbed spatial subdomain is fixed to material 1. Table II shows the flux difference resulting from the perturbation in cube 1 from material 2 to material 3. Here, P1 corresponds to material 2 in cube 1 and P2 material 3 in cube 1. It

TABLE I
Three Energy Group Macroscopic Cross Sections in cm^{-1} with Isotropic Scattering

	Material number j			
	1	2	3	4
$\Sigma_{j,t,1}$	0.333333	0.333333	0.333333	0.333333
$\Sigma_{j,t,2}$	0.5	0.5	0.5	0.5
$\Sigma_{j,t,3}$	0.666666	0.666666	0.666666	0.666666
$\Sigma_{j,s,1}$	0.326666	0.3	0.283333	0.166666
$\Sigma_{j,s,2}$	0.49	0.45	0.425	0.25
$\Sigma_{j,s,3}$	0.653333	0.6	0.566666	0.333333
$\Sigma_{j,s,1\to1}$	0.294	0.27	0.255	0.15
$\Sigma_{j,s,1\to2}$	0.032666	0.03	0.028333	0.016666
$\Sigma_{j,s,2\to2}$	0.441	0.405	0.3825	0.225
$\Sigma_{j,s,2\to3}$	0.049000	0.045	0.0425	0.025
$\Sigma_{j,s,3\to3}$[a]	0.653333	0.6	0.566666	0.333333

[a] Other group transfer macroscopic cross sections are zero.

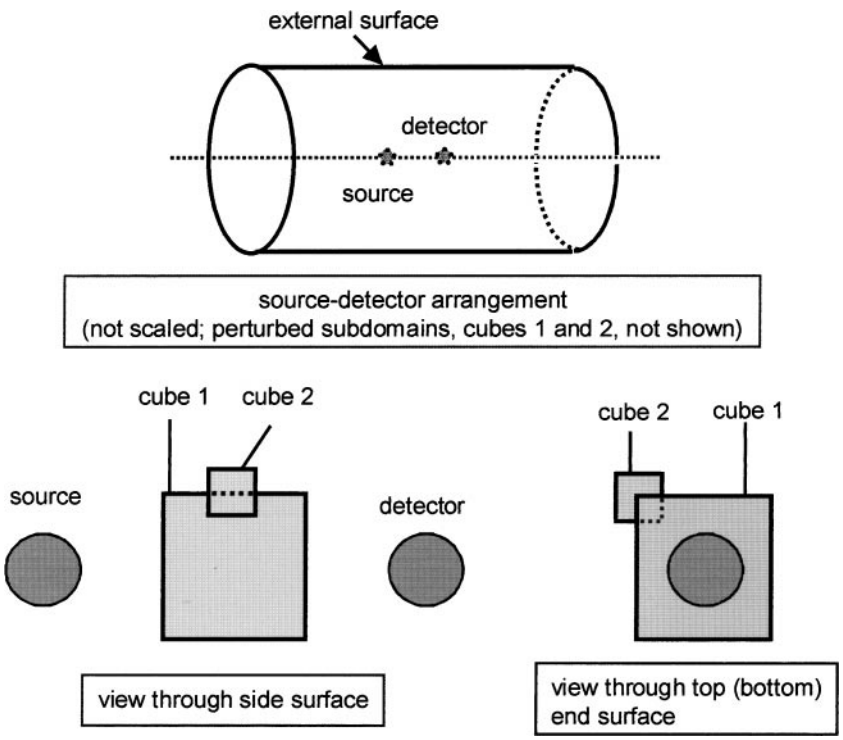

FIG. 3. Arrangement of source, detector, and perturbed spatial subdomains for three energy group problems. (The whole spatial domain is a cylinder with 45 cm radius and 90 cm length; the source and detector are sphere with 1.5 cm radius, and their centers lie on the cylinder axis and are separated by 16 cm and away from the top and bottom surfaces by equal distances; either cube 1 or 2 is a materially perturbed subdomain as in (b) in Fig. 1; the center of cube 1 lies at the midpoint of the centers of the source and detector; the side of cube 1 is 6 cm; two surfaces of cube 1 are vertical to the cylinder axis; any of the surfaces of cube 2 are parallel to some of the surfaces of cube 1; the side of cube 2 is 2 cm; the center of cube 2 lies at the midpoint of one of the sides of cube 1 as drawn above.)

TABLE II
Flux Difference (cm^{-2} s^{-1}) Resulting from the Perturbation from Material 2 to Material 3 inside Cube 1

	Difference of two independent standard forward calculations	Correlated coupling
First group	7.28×10^{-6}	5.90×10^{-6}
	(0.103)[a]	(0.110)[a]
Second group	8.77×10^{-6}	8.19×10^{-6}
	(0.071)[a]	(0.060)[a]
Third group	5.16×10^{-5}	5.03×10^{-5}
	(0.022)[a]	(0.016)[a]
cpu time (min.)[b]	10366[c]	3870[d]

Note. Material 1 outside cube 1; first group particle source; flux is normalized per particle born at source.

[a] Fractional standard deviation.

[b] Measured by Digital AlphaStation 600 5.

[c] $2 \times 100{,}000{,}000$ histories.

[d] 20,000,000 initial variable samplings based on Eq. (32); 4 adjoint and 2×40 forward histories per initial variable.

can be observed that the computed values agree very well. Overall, correlated coupling is about three times as efficient as taking the difference of two standard forward calculations. Table III shows the flux difference resulting from the perturbation in cube 2 from material 2 to material 4. Here, P1 corresponds to material 2 in cube 2 and P2 material 4 in cube 2. It can be observed that the results from taking the difference between two independent forward calculations are hopelessly inefficient for the first and second energy groups, while all the results in correlated coupling have fractional standard deviations of

TABLE III
Flux Difference (cm^{-2} s^{-1}) Resulting from the Perturbation from Material 2 to Material 4 inside Cube 2

	Difference of two independent standard forward calculations	Correlated coupling
First group	8.33×10^{-8}	1.47×10^{-6}
	(12.6)[a]	(0.046)[a]
Second group	1.90×10^{-6}	1.70×10^{-6}
	(0.467)[a]	(0.036)[a]
Third group	1.68×10^{-5}	1.56×10^{-5}
	(0.106)[a]	(0.009)[a]
cpu time (min.)[b]	6341[c]	2742[d]

Note. Material 1 outside cube 2; first group particle source; flux is normalized per particle born at source.

[a] Fractional standard deviation.

[b] Measured by Digital AlphaStation 600 5.

[c] $2 \times 60{,}000{,}000$ histories.

[d] 10,000,000 initial variable samplings based on Eq. (32); 4 adjoint and 2×40 forward histories per initial variable.

TABLE IV
Materials for 30 Energy Group Calculations

Material 5:	limestone with 20% porosity, 2.3688 g/cm^3
Material 6:	Si : O : H : Na : Cl = 0.360 : 0.590 : 0.022 : 0.011 : 0.017 in wt%, 2.3g/cm^3
Material 7:	water (H_2O), 1.0 g/cm^3
Material 8:	steel (Fe), 7.86 g/cm^3
Material 9:	helium 3 gas (He^3), 0.000502 g/cm^3

less than 5% with less than half the cpu time of those forward calculations. The results in Tables II and III suggest that perturbation analysis by correlated coupling can be a very valuable tool for perturbation in a small spatial subdomain isolated from the source and detector.

Table IV shows materials used in 30 group calculations. Nuclear cross section library accompanied with the MCNP code was used for those materials. Figure 4 shows the material distribution and source-detector enclosure. An isotropic americium–beryllium neutron source embedded in steel is considered. Material 5 is changed to material 6 and the difference of the total flux averaged over the detector volume is calculated. Here, P1 corresponds to material 5 outside the right parallelepiped and P2 material 6 outside that parallelpiped. The material distribution inside the the right parallelepiped is fixed as shown in Fig. 4. Table V shows numerical results for total neutron flux difference. The results from correlated coupling agree very well with those from two independent standard forward calculations. The computation of Eq. (31) is much more efficient than two independent standard forward calculations, while the computation of Eq. (30) is inefficient. Since the computational domain of the succeeding simulations is much larger than that of the preceding simulation, the succeeding simulations should have the larger of the physical source and detector as their simulation detector. Here, a simulation detector is intended to stand for a physical detector in forward simulations or a physical source in adjoint simulations. In the case of Fig. 4, adjoint simulations should be chosen as the succeeding simulations, which implies the computation of Eq. (31).

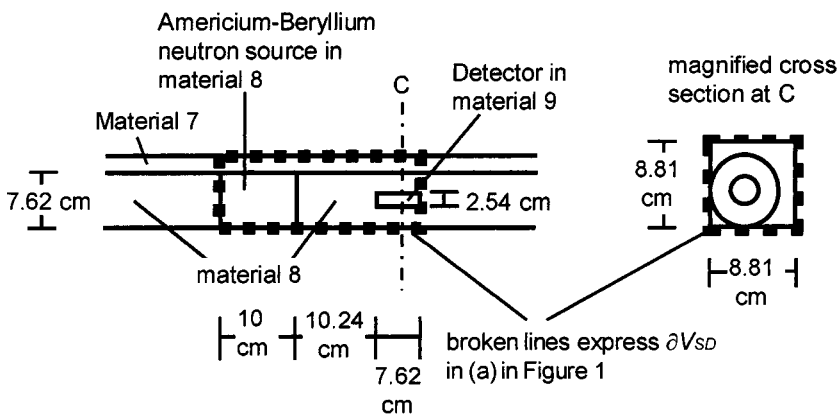

FIG. 4. Infinite medium of material 5 with right parallelepiped of infinite length containing different materials (material 5 not shown; broken lines show the source-detector enclosure).

TABLE V

Total Neutron Flux Difference (cm^{-2} s^{-1}) Resulting from the Perturbation outside the Right Parallelepiped in Fig. 4 from Material 5 to Material 6 in Table IV

	Difference of two independent standard forward calculations	Correlated coupling	
		Eq. (30)	Eq. (31)
Flux Difference	-1.143×10^{-4}	-1.107×10^{-4}	-1.165×10^{-4}
FSD[a]	0.0095	0.0382	0.0107
cpu time (min)[b]	11246[c]	1564[d]	1509[e]

[a] Fractional standard deviation.

[b] Measured by Digital AlphaStation 600 5.

[c] $2 \times 80{,}000{,}000$ histories.

[d] 960,000 initial variable samplings based on Eq. (32); 4 adjoint and 2×40 forward histories per initial variable.

[e] 10,000,000 initial variable samplings based on Eq. (34); 4 forward and 2×40 adjoint histories per initial variable.

V. SUMMARY AND DISCUSSION

This paper has investigated a neutron or photon transport problem with perturbing material outside a subdomain containing both the source and detector. Monte Carlo correlated coupling has been developed which computes the variation of the detector response by initiating forward and adjoint histories in opposite directions at the surface of the perturbing material. One history simulates the trajectory in the unperturbed subdomain and the other history simulates the trajectory traversing the perturbed subdomain. In principle, the latter simulation can be applied to many material changes in the perturbed subdomain and can be coupled with just the single former simulation to compute the corresponding response variations. The advantageous points of the method developed are summarized as follows. First, the procedure of taking the difference between the results from two independent calculations after the completion of all the histories is avoided with no approximation. The method is based on the unbiased estimation of the exact surface integral expression of the response variation. Second, the statistical error of the response variation is estimated in the same way as in the confidence interval estimation in a standard forward or adjoint simulation. Usually, these two points are not simultaneously satisfied by standard techniques in Monte Carlo perturbation analysis [9, 10]. Thus, the methodology developed in Section III may complement conventional practices. There are three immediate possibilities for further developments:

1. The application to neutron and photon coupled transport can be investigated by extending the perturbation analysis in Section III to the coupled transport equations with neutron and photon fluxes.

2. Conventional perturbation analysis techniques such as differential operator sampling and correlated sampling [3, 9, 10, 12] may be combined with correlated coupling. An attempt can be made at applying these techniques to the forward or adjoint history simulating the trajectory traversing a perturbed subdomain. Batch-average product processing [7] should be utilized as in the numerical results in Section IV.

3. The correlated coupling in this paper can be combined with next-event estimation coupling in the generalized coupled history [6]. Figure 5 schematically shows a procedure

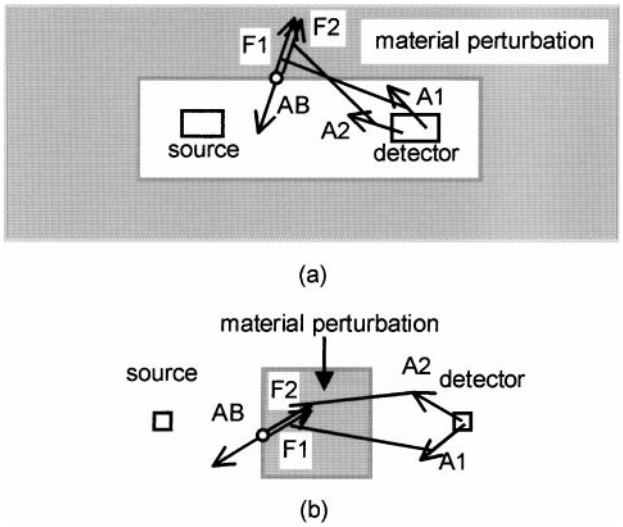

FIG. 5. Next-event estimation coupling for perturbation analysis. ["F1" and "F2" imply the forward histories in Figure 2; "AB" implies the adjoint hisotry in Figure 2; material in the perturbed subdomain is made purely absorbing for the independent adjoint histories "A1" and "A2" starting from the detector; next-event estimation couples collision sites in F1 with those in A1 to estimate $\Psi_1^*(\underline{r}_1, \underline{\Omega}_l, E_1)$ and collision sites in F2 with those in A2 to estimate $\Psi_2^*(\underline{r}_1, \underline{\Omega}_l, E_1)$.)

to do it. Perturbation invariance (an unbiased perturbation method of midway response) in previous work [4, 7] should be applied to improve the next-event estimation using a purely absorbing material [21]. In principle, a physical particle history is divided into three parts: (1) the trajectory from the birth to the first entrance into a perturbed subdomain, (2) the trajectory toward a detector after the last exit from the perturbed subdomain, and (3) the trajectory in between. The response decomposition in this paper separates (1) from (2) and (3), or (2) from (1) and (3). The perturbation invariance with a purely absorbing material divides the remaining trajectories. Correlated coupling and next-event estimation coupling couple (1) with (2) and (2) with (3).

APPENDIX A

Three Formally Adjoint Equations Corresponding to Sampled Initial Variables

Suppose that $(\underline{r}_I, \Omega_I, E_I)$ are initial variables sampled from the probability density function $f(\underline{r}, E)\underline{n} \cdot \Omega/\pi$ over $\partial V_{SD} \backslash \partial V$, the positive half of the unit spherical surface at the origin and $(0, E_0)$. The formally adjoint equations to estimate $\Psi_B(\underline{r}_I, \Omega_I, E_I)$, $\Psi_1^*(\underline{r}_I, \Omega_I, E_I)$ and $\Psi_2^*(\underline{r}_I, \Omega_I, E_I)$ are presented in this appendix.

The formally adjoint equation to estimate $\Psi_B(\underline{r}_I, \Omega_I, E_I)$ is

$$-\Omega \cdot \nabla \Phi_B^*(\underline{r}, \Omega, E) + \Sigma_t(\underline{r}, E)\Phi_B^*(\underline{r}, \Omega, E)$$
$$= \int_0^{E_0} \int_{4\pi} \Sigma_s(\underline{r}, \Omega \to \Omega', E \to E')\Phi_B^*(\underline{r}, \Omega', E')\, d\Omega'\, dE' \quad \text{for } \underline{r} \in \mathbf{V}_{SD}, \quad \text{(A.1)}$$

$$\Phi_B^*(\mathbf{r}, \Omega, E) = \delta[\partial V_{SD} \backslash \partial V](\mathbf{r} - \mathbf{r}_I)\delta(E - E_I)\frac{\delta_2(\Omega - \Omega_I)}{\mathbf{n} \cdot \Omega_I}$$
$$\text{for } \mathbf{r} \in \partial V_{SD} \backslash \partial V \text{ and } \Omega \cdot \mathbf{n} > 0, \tag{A.2}$$

$$\Phi_B^*(\mathbf{r}, \Omega, E) = 0 \quad \text{for } \mathbf{r} \in \partial V_{SD} \cap \partial V \text{ and } \Omega \cdot \mathbf{n} > 0, \tag{A.3}$$

where $\delta[\partial V_{SD} \backslash \partial V](\mathbf{r} - \mathbf{r}_I)$ is the Dirac delta function on $\partial V_{SD} \backslash \partial V$, $\delta_2(\Omega - \Omega_I)$ is the Dirac delta function on the unit spherical surface at the origin, and Eq. (A.3) is intended to treat (b) in Fig. 1. (The set $\partial V_{SD} \cap \partial V$ is an empty set for (a) in Fig. 1.) Following steps similar to those leading to Eq. (7), Eqs. (21) and (22), and (A.1)–(A.3) yield

$$\Psi_B(\mathbf{r}_I, \Omega_I, E_I) = \int_{V_{SD}} \int_{4\pi} \int_0^{E_0} S(\mathbf{r}, \Omega, E)\Phi_B^*(\mathbf{r}, \Omega, E)\, dE\, d\Omega\, dV. \tag{A.4}$$

Equation (A.4) implies that the Monte Carlo simulation of Eqs. (A.1)–(A.3) estimates $\Psi_B(\mathbf{r}_I, \Omega_I, E_I)$.

The formally adjoint equation to estimate $\Psi_1^*(\mathbf{r}_I, \Omega_I, E_I)$ is

$$\Omega \cdot \nabla\Phi_1(\mathbf{r}, \Omega, E) + \Sigma_t(\mathbf{r}, E)\Phi_1(\mathbf{r}, \Omega, E)$$
$$= \int_0^{E_0} \int_{4\pi} \Sigma_s(\mathbf{r}, \Omega' \to \Omega, E' \to E)\Phi_1(\mathbf{r}, \Omega', E')\, d\Omega'\, dE' \quad \text{for } \mathbf{r} \in V_{SD}, \tag{A.5}$$

$$\Omega \cdot \nabla\Phi_1(\mathbf{r}, \Omega, E) + \Sigma_{1,t}(\mathbf{r}, \Omega, E)\Phi_1(\mathbf{r}, \Omega, E)$$
$$= \int_0^{E_0} \int_{4\pi} \Sigma_{1,s}(\mathbf{r}, \Omega' \to \Omega, E' \to E)\Phi_1(\mathbf{r}, \Omega', E')\, d\Omega'\, dE' \quad \text{for } \mathbf{r} \in V \backslash V_{SD}, \tag{A.6}$$

$$\Phi_1(\mathbf{r}, \Omega, E) = 0 \quad \text{for } \mathbf{r} \in \partial V \text{ and } \Omega \cdot \mathbf{n} < 0, \tag{A.7}$$

$$\lim_{\epsilon \downarrow 0} \mathbf{n} \cdot \Omega\Phi_1(\mathbf{r} + \epsilon\Omega, \Omega, E) - \lim_{\epsilon \downarrow 0} \mathbf{n} \cdot \Omega\Phi_1(\mathbf{r} - \epsilon\Omega, \Omega, E)$$
$$= \delta[\partial V_{SD} \backslash \partial V](\mathbf{r} - \mathbf{r}_I)\delta(E - E_I)\delta_2(\Omega - \Omega_I)$$
$$\text{for } \mathbf{r} \in \partial V_{SD} \backslash \partial V \text{ and } \Omega \cdot \mathbf{n} > 0, \tag{A.8}$$

$$\lim_{\epsilon \downarrow 0} \Phi_1(\mathbf{r} + \epsilon\Omega, \Omega, E)$$
$$= \lim_{\epsilon \downarrow 0} \Phi_1(\mathbf{r} - \epsilon\Omega, \Omega, E) \quad \text{for } r \in \partial V_{SD} \backslash \partial V \text{ and } \Omega \cdot \mathbf{n} < 0, \tag{A.9}$$

where in Eq. (A.8), the unit monoenergetic and monodirectional point source resulting from $(\mathbf{r}_I, \Omega_I, E_I)$ is expressed as a current jump condition. By considering the spatial integral over an intertal volume strictly contained inside V_{SD} and letting its surface overlap ∂V_{SD} from the negative side of ∂V_{SD}, Eqs. (11), (13) and (A.5), (A.7) yield

$$-\int_{V_{SD}} \int_{4\pi} \int_0^{E_0} D(\mathbf{r}, \Omega, E)\Phi_1(\mathbf{r}, \Omega, E)\, dE\, d\Omega\, dV$$
$$= \int_{\mathbf{n}\cdot\Omega>0} \int_{\partial V_{SD} \backslash \partial V} \int_0^{E_0} \mathbf{n} \cdot \Omega \lim_{\epsilon \downarrow 0} \Phi_1(\mathbf{r} - \epsilon\Omega, \Omega, E)\Psi_1^*(\mathbf{r}, \Omega, E)\, dE\, dA\, d\Omega$$
$$+ \int_{\mathbf{n}\cdot\Omega<0} \int_{\partial V_{SD} \backslash \partial V} \int_0^{E_0} \mathbf{n} \cdot \Omega \lim_{\epsilon \downarrow 0} \Phi_1(\mathbf{r} + \epsilon\Omega, \Omega, E)\Psi_1^*(\mathbf{r}, \Omega, E)\, dE\, dA\, d\Omega. \tag{A.10}$$

By considerling the spatial integral over an internal volume strictly containing V_{SD} and letting its external surface overlap ∂V_{SD} from the positive side of $\partial V_{SD} \backslash \partial V$, Eqs. (11)–(13) and (A.5)–(A.9) yield

$$0 = \int_{n\cdot\Omega>0} \int_{\partial V_{SD}\backslash\partial V} \int_0^{E_0} n\cdot\Omega \lim_{\epsilon\downarrow 0} \Phi_1(r+\epsilon\Omega,\Omega,E)\Psi_1^*(r,\Omega,E)\,dE\,dA\,d\Omega + \int_{n\cdot\Omega<0} \int_{\partial V_{SD}\backslash\partial V} \int_0^{E_0} n\cdot\Omega \lim_{\epsilon\downarrow 0} \Phi_1(r-\epsilon\Omega,\Omega,E)\Psi_1^*(r,\Omega,E)\,dE\,dA\,d\Omega, \quad \text{(A.11)}$$

where the left-hand side is zero because the volume that is shrinking to V_{SD} contains both the source and detector, and the so-called contributions represented by $\Phi_1\Psi_1^*$ originate at the source, flow out at the detector, do not leak through the the external surface ∂V, and survive a collision with probability one and no multiplication [12]. The current jump condition (A.8) with the continuity of $\Psi_2^*(r,\Omega,E)$ yields

$$\int_{n\cdot\Omega>0} \int_{\partial V_{SD}\backslash\partial V} \int_0^{E_0} n\cdot\Omega \lim_{\epsilon\downarrow 0} \Phi_1(r-\epsilon\Omega,\Omega,E)\Psi_1^*(r,\Omega,E)\,dE\,dA\,d\Omega + \Psi_1^*(r_I,\Omega_I,E_I) = \int_{n\cdot\Omega>0} \int_{\partial V_{SD}\backslash\partial V} \int_0^{E_0} n\cdot\Omega \lim_{\epsilon\downarrow 0} \Phi_1(r+\epsilon\Omega,\Omega,E)\Psi_1^*(r,\Omega,E)\,dE\,dA\,d\Omega, \quad \text{(A.12)}$$

and Eq. (A.9) yields

$$\int_{n\cdot\Omega<0} \int_{\partial V_{SD}\backslash\partial V} \int_0^{E_0} n\cdot\Omega \lim_{\epsilon\downarrow 0} \Phi_1(r+\epsilon\Omega,\Omega,E)\Psi_1^*(r,\Omega,E)\,dE\,dA\,d\Omega = \int_{n\cdot\Omega<0} \int_{\partial V_{SD}\backslash\partial V} \int_0^{E_0} n\cdot\Omega \lim_{\epsilon\downarrow 0} \Phi_1(r-\epsilon\Omega,\Omega,E)\Psi_1^*(r,\Omega,E)\,dE\,dA\,d\Omega. \quad \text{(A.13)}$$

Adding Eq. (A.13) to Eq. (A.12) side by side and using Eq. (A.11), one obtains

$$\int_{n\cdot\Omega>0} \int_{\partial V_{SD}\backslash\partial V} \int_0^{E_0} n\cdot\Omega \lim_{\epsilon\downarrow 0} \Phi_1(r-\epsilon\Omega,\Omega,E)\Psi_1^*(r,\Omega,E)\,dE\,dA\,d\Omega + \int_{n\cdot\Omega<0} \int_{\partial V_{SD}\backslash\partial V} \int_0^{E_0} n\cdot\Omega \lim_{\epsilon\downarrow 0} \Phi_1(r+\epsilon\Omega,\Omega,E)\Psi_1^*(r,\Omega,E)\,dE\,dA\,d\Omega + \Psi_1^*(r_I,\Omega_I,E_I) = 0. \quad \text{(A.14)}$$

Equations (A.10) and (A.14) yield

$$\Psi_1^*(r_I,\Omega_I,E_I) = \int_{V_{SD}} \int_{4\pi} \int_0^{E_0} D(r,\Omega,E)\Phi_1(r,\Omega,E)\,dE\,d\Omega\,dV. \quad \text{(A.15)}$$

Equations (A.15) implies that the Monte Carlo simulation of Eqs. (A.5)–(A.9) estimates $\Psi_1^*(r_I,\Omega_I,E_I)$.

The formally adjoint equation to estimate $\Psi_2^*(r_I, \Omega_I, E_I)$ is

$$\Omega \cdot \nabla \Phi_2(r, \Omega, E) + \Sigma_t(r, E)\Phi_2(r, \Omega, E) = \int_0^{E_0} \int_{4\pi} \Sigma_s(r, \Omega' \to \Omega, E' \to E)\Phi_2(r, \Omega', E')\, d\Omega'\, dE' \quad \text{for } r \in V_{SD}, \tag{A.16}$$

$$\Omega \cdot \nabla \Phi_2(r, \Omega, E) + \Sigma_{2,t}(r, \Omega, E)\Phi_2(r, \Omega, E) = \int_0^{E_0} \int_{4\pi} \Sigma_{2,s}(r, \Omega' \to \Omega, E' \to E)\Phi_2(r, \Omega', E')\, d\Omega'\, dE' \quad \text{for } r \in V \backslash V_{SD}, \tag{A.17}$$

$$\Phi_2(r, \Omega, E) = 0 \quad \text{for } r \in \partial V \text{ and } \Omega \cdot n < 0, \tag{A.18}$$

$$\lim_{\epsilon \downarrow 0} n \cdot \Omega \Phi_2(r + \epsilon\Omega, \Omega, E) - \lim_{\epsilon \downarrow 0} n \cdot \Omega \Phi_2(r - \epsilon\Omega, \Omega, E) = \delta[\partial V_{SD} \backslash \partial V](r - r_I)\delta(E - E_I)\delta_2(\Omega - \Omega_I) \quad \text{for } r \in \partial V_{SD} \backslash \partial V \text{ and } \Omega \cdot n > 0, \tag{A.19}$$

$$\lim_{\epsilon \downarrow 0} \Phi_2(r + \epsilon\Omega, \Omega, E) = \lim_{\epsilon \downarrow 0} \Phi_2(r - \epsilon\Omega, \Omega, E) \quad \text{for } r \in \partial V_{SD} \backslash \partial V \text{ and } \Omega \cdot n < 0. \tag{A.20}$$

Through manipulation in the same way as in Eqs. (A.5)–(A.15), one obtains

$$\Psi_2^*(r_I, \Omega_I, E_I) = \int_{V_{SD}} \int_{4\pi} \int_0^{E_0} D(r, \Omega, E)\Phi_2(r, \Omega, E)\, dE\, d\Omega\, dV. \tag{A.21}$$

Eq. (A.21) implies that the Monte Carlo simulation of Eqs. (A.16)–(A.20) estimates $\Psi_2^*(r_I, \Omega_I, E_I)$.

APPENDIX B

Response Variation Resulting from Material Change Separating a Source and a Detector and Its Relation to the Adjoint Difference Method

Response variation because of material changes in a subdomain separating a source and a detector is considered. In other words, a case wherein any source-detector enclosure contains part of the perturbed subdomain is considered. The relation to the adjoint difference method [14] is also described. First, the source is assumed to be situated outside the perturbed subdomain. The forward transport equation for an unperturbed subdomain containing the source is

$$\Omega \cdot \nabla \eta(r, \Omega, E) + \Sigma_t(r, E)\eta(r, \Omega, E) = \int_0^{E_0} \int_{4\pi} \Sigma_s(r, \Omega' \to \Omega, E' \to E)\eta(r, \Omega', E')\, d\Omega'\, dE' + S(r, \Omega, E) \quad \text{for } r \in V_S, \tag{B.1}$$

$$\eta(r, \Omega, E) = 0 \quad \text{for } r \in \partial V_S \text{ and } \Omega \cdot n < 0. \tag{B.2}$$

The adjoint transport equation for the whole spatial domain is

$$-\Omega \cdot \nabla \eta_i^*(r, \Omega, E) + \Sigma_t(r, E)\eta_i^*(r, \Omega, E)$$
$$= \int_0^{E_0} \int_{4\pi} \Sigma_s(r, \Omega \to \Omega', E \to E')\eta_i^*(r, \Omega', E')\, d\Omega'\, dE', \quad \text{for } r \in V_S, \tag{B.3}$$
$$-\Omega \cdot \nabla \eta_i^*(r, \Omega, E) + \Sigma_{i,t}(r, \Omega, E)\eta_i^*(r, \Omega, E)$$
$$= \int_0^{E_0} \int_{4\pi} \Sigma_{i,s}(r, \Omega \to \Omega', E \to E')\eta_i^*(r, \Omega', E')\, d\Omega'\, dE' + D(r, \Omega, E) \quad \text{for } r \in V_D, \tag{B.4}$$

$$\eta_i^*(r, \Omega, E) = 0 \quad \text{for } r \in \partial V \text{ and } \Omega \cdot n > 0, \tag{B.5}$$

with a continuity condition at the internal boundary,

$$\lim_{\epsilon \downarrow 0} \eta_i^*(r - \epsilon\Omega, \Omega, E) = \lim_{\epsilon \downarrow 0} \eta_i^*(r + \epsilon\Omega, \Omega, E) \quad \text{for } r \in \partial V_S \cap \partial V_D,$$

where the subscript i of the macroscopic cross sections in Eq. (B.4) implies that any material designated as i can occupy V_D, the subscript i of the adjoint flux stands for the corresponding solution, the whole spatial domain V is divided into V_S and V_D, $S = 0$ in V_D, and $D = 0$ in V_S. Note that the material in V_S is the same for both the forward and adjoint equations, and the perturbation is relegated to the arbitrariness of material i. By the black absorber technique [4, 7], the detector response due to the material i has two expressions in terms of $\eta(r, \Omega, E)$ and $\eta_i^*(r, \Omega, E)$:

$$R_i = \int_{V_S} \int_{4\pi} \int_0^{E_0} S(r, \Omega, E)\eta_i^*(r, \Omega, E)\, dE\, d\Omega\, dV$$
$$= \int_{\partial V_S \cap \partial V_D} \int_{n \cdot \Omega > 0} \int_0^{E_0} n \cdot \Omega \eta(r, \Omega, E)\eta_i^*(r, \Omega, E)\, dE\, d\Omega\, dA. \tag{B.6}$$

The response variation resulting from the material change from $i = 1$ to $i = 2$ is expressed as

$$R_2 - R_1 = \int_{\partial V_S \cap \partial V_D} \int_{n \cdot \Omega > 0} \int_0^{E_0} n \cdot \Omega \eta(r, \Omega, E)[\eta_2^*(r, \Omega, E)$$
$$- \eta_1^*(r, \Omega, E)]\, dE\, d\Omega\, dA. \tag{B.7}$$

This can be handled as in Eq. (32).

Second, the detector is assumed to be situated outside the perturbed subdomain. The adjoint transport equation for an unperturbed subdomain containing the detector is

$$-\Omega \cdot \nabla \xi^*(r, \Omega, E) + \Sigma_t(r, E)\xi^*(r, \Omega, E)$$
$$= \int_0^{E_0} \int_{4\pi} \Sigma_s(r, \Omega \to \Omega', E \to E')\xi^*(r, \Omega', E')\, d\Omega'\, dE'$$
$$+ D(r, \Omega, E) \quad \text{for } r \in V_D, \tag{B.8}$$
$$\xi^*(r, \Omega, E) = 0 \quad \text{for } r \in \partial V_D \text{ and } \Omega \cdot n > 0. \tag{B.9}$$

The forward transport equation for the whole spatial domain is

$$\Omega \cdot \nabla \xi_i(r, \Omega, E) + \Sigma_t(r, E)\xi_i(r, \Omega, E)$$
$$= \int_0^{E_0} \int_{4\pi} \Sigma_s(r, \Omega' \to \Omega, E' \to E)\xi_i(r, \Omega', E')\, d\Omega'\, dE', \quad \text{for } r \in V_D, \tag{B.10}$$

$$\Omega \cdot \nabla \xi_i(r, \Omega, E) + \Sigma_{i,t}(r, \Omega, E)\xi_i(r, \Omega, E)$$
$$= \int_0^{E_0} \int_{4\pi} \Sigma_{i,s}(r, \Omega' \to \Omega, E' \to E)\xi_i(r, \Omega', E')\, d\Omega'\, dE' + S(r, \Omega, E) \quad \text{for } r \in V_S, \tag{B.11}$$

$$\xi_i(r, \Omega, E) = 0 \quad \text{for } r \in \partial V \text{ and } \Omega \cdot n < 0, \tag{B.12}$$

with a continuity condition

$$\lim_{\epsilon \downarrow 0} \xi_i(r - \epsilon\Omega, \Omega, E) = \lim_{\epsilon \downarrow 0} \xi_i(r + \epsilon\Omega, \Omega, E) \quad \text{for } r \in \partial V_S \cap \partial V_D.$$

By the black absorber technique [4, 7], the detector response resulting from the material i has two expressions in terms of $\xi^*(r, \Omega, E)$ and $\xi_i(r, \Omega, E)$,

$$R_i = \int_{V_D} \int_{4\pi} \int_0^{E_0} D(r, \Omega, E)\xi_i(r, \Omega, E)\, dE\, d\Omega\, dV$$
$$= -\int_{\partial V_S \cap \partial V_D} \int_{n \cdot \Omega < 0} \int_0^{E_0} n \cdot \Omega \xi_i(r, \Omega, E)\xi^*(r, \Omega, E)\, dE\, d\Omega\, dA, \tag{B.13}$$

where the positive directions of $\partial V_S \cap \partial V_D$ in Eqs. (B.6) and (B.13) are opposite. The second equality in Eq. (B.13) is equivalent to Eq. (15) in the work of Hoffman *et al.* [14]. The response variation resulting from the material change from $i = 1$ to $i = 2$ is expressed as

$$R_2 - R_1 = -\int_{\partial V_S \cap \partial V_D} \int_{n \cdot \Omega < 0} \int_0^{E_0} n \cdot \Omega[\xi_2(r, \Omega, E) - \xi_1(r, \Omega, E)]$$
$$\times \xi^*(r, \Omega, E)\, dE\, d\Omega\, dA. \tag{B.14}$$

This can be handled as in Eq. (34). Now, we perturb the common macroscopic cross sections in V_D for the adjoint equations (B.8) and (B.9)

$$-\Omega \cdot \nabla \tilde{\xi}^*(r, \Omega, E) + \tilde{\Sigma}_t(r, E)\tilde{\xi}^*(r, \Omega, E)$$
$$= \int_0^{E_0} \int_{4\pi} \tilde{\Sigma}_s(r, \Omega \to \Omega', E \to E')\tilde{\xi}^*(r, \Omega', E')\, d\Omega'\, dE' + D(r, \Omega, E) \quad \text{for } r \in V_D, \tag{B.15}$$

$$\tilde{\xi}^*(r, \Omega, E) = 0 \quad \text{for } r \in \partial V_D \text{ and } \Omega \cdot n > 0, \tag{B.16}$$

and the forward equations (B.10)–(B.12)

$$\Omega \cdot \nabla \tilde{\xi}_i(r, \Omega, E) + \tilde{\Sigma}_t(r, E)\tilde{\xi}_i(r, \Omega, E)$$
$$= \int_0^{E_0} \int_{4\pi} \tilde{\Sigma}_s(r, \Omega' \to \Omega, E' \to E)\tilde{\xi}_i(r, \Omega', E')\, d\Omega'\, dE', \quad \text{for } r \in V_D, \tag{B.17}$$

$$\Omega \cdot \nabla \tilde{\xi}_i(r, \Omega, E) + \Sigma_{i,t}(r, \Omega, E)\tilde{\xi}_i(r, \Omega, E)$$
$$= \int_0^{E_0} \int_{4\pi} \Sigma_{i,s}(r, \Omega' \to \Omega, E' \to E)\tilde{\xi}_i(r, \Omega', E')\, d\Omega'\, dE' + S(r, \Omega, E) \quad \text{for } r \in V_S, \tag{B.18}$$

$$\tilde{\xi}_i(r, \Omega, E) = 0 \quad \text{for } r \in \partial V \text{ and } \Omega \cdot n < 0, \tag{B.19}$$

where the continuity condition of ξ_i holds for $\tilde{\xi}_i$ as well. The perturbed detector response resulting from the material i is expressed as in Eq. (B.13) by

$$\tilde{R}_i = \int_{V_D} \int_{4\pi} \int_0^{E_0} D(r, \Omega, E)\tilde{\xi}_i(r, \Omega, E)\, dE\, d\Omega\, dV$$
$$= -\int_{\partial V_S \cap \partial V_D} \int_{n\cdot\Omega<0} \int_0^{E_0} n \cdot \Omega \tilde{\xi}_i(r, \Omega, E)\tilde{\xi}^*(r, \Omega, E)\, dE\, d\Omega\, dA. \tag{B.20}$$

When V_D is small compared to the whole spatial domain and the source and detector are separated by large distance, $\tilde{R}_i$ may be approximated as

$$\tilde{R}_i \approx -\int_{\partial V_S \cap \partial V_D} \int_{n\cdot\Omega<0} \int_0^{E_0} n \cdot \Omega \xi_i(r, \Omega, E)\tilde{\xi}^*(r, \Omega, E)\, dE\, d\Omega\, dA. \tag{B.21}$$

This is called the surface integral approximation [14]. Its associate error is

$$\Delta\tilde{R}_i = \int_{\partial V_S \cap \partial V_D} \int_{n\cdot\Omega<0} \int_0^{E_0} n \cdot \Omega[\xi_i(r, \Omega, E) - \tilde{\xi}_i(r, \Omega, E)]$$
$$\times \tilde{\xi}^*(r, \Omega, E)\, dE\, d\Omega\, dA. \tag{B.22}$$

This was proven to be equal to the error associated with the adjoint difference approximation [14].

REFERENCES

1. K. M. Case and P. F. Zweifel, *Linear Transport Theory* (Addison-Wesley, Reading, MA, 1967).
2. B. Eriksson et al., Monte Carlo integration of the adjoint neutron transport equation, *Nucl. Sci. Eng.* **37**, 410 (1969).
3. I. Lux and L. Koblinger, *Monte Carlo Particle Transport Methods: Neutron and Photon Calculations* (CRC Press, Boca Raton, FL, 1991).
4. I. V. Serov, T. M. John, and J. E. Hoogenboom, A midway forward-adjoint coupling method for neutron and photon Monte Carlo transport, *Nucl. Sci. Eng.* **133**, 55 (1999).
5. Y. Hayashida et al., Development of Sn-AMC-AMC Coupling Technique and Its Application to Analysis of Neutron Streaming Data of 'JOYO', *J. Nucl. Sci. Tech.* **24** (2), 89 (1987).
6. S. N. Cramer, Forward-adjoint Monte Carlo coupling with no statistical error propagation, *Nucl. Sci. Eng.* **124**, 398 (1996).
7. T. Ueki, J. E. Hoogenboom, and J. L. Kloosterman, Analysis of correlated coupling of Monte Carlo forward and adjoint histories, *Nucl. Sci. Eng.* **137**, 117 (2001).
8. T. Ueki and J. E. Hoogenboom, Particle reflection in correlated coupling of Monte Carlo forward and adjoint histories, in *CD-ROM Proceedings of the PHYSOR 2000*, *ANS International Topical Meeting on Advances in Reactor Physics and Mathematics and Computation into the Next Millennium*, *Pittsburgh Pennsylvania*, *May 7–11, 2000* (Am. Nuclear Soc. La Grange Park, IL, 2000).

9. H. Rief, Generalized Monte Carlo perturbation algorithms for correlated sampling and a second-order Taylor series approach, *Ann. Nucl. Energy* **11**, 455 (1984).
10. H. Rief, A synopsis of Monte Carlo perturbation algorithms, *J. Comput. Phys.* **111**, 33 (1994).
11. G. I. Bell and S. I. Glasstone, *Nuclear Reactor Theory*, (Krieger Malabar, FL, 1985).
12. M. L. Williams, Generalized contributon response theory, *Nucl. Sci. Eng*. **108**, 355 (1991).
13. G. B. Folland, *Real Analysis*, 2nd ed. (Wiley New York, 1999).
14. T. J. Hoffman, J. C. Robinson, and P. N. Stevens, The adjoint difference method and its application to deep-penetration radiation transport, *Nucl. Sci. Eng*. **48**, 179 (1972).
15. R. Sánchez, Duality, Green's functions and all that, *Transp. Theory Stat. Phys.* **27**(5–7), 445 (1998).
16. M. Lòeve, *Probability Theory II*, 4th ed. (Springer-Verlag, New York, 1978).
17. P. Billingsley, *Probability and Measure*, 3rd. ed. (Wiley, New York, 1995).
18. J. E. Hoogenboom,Continuous energy adjoint Monte Carlo in MCNP with minor code extensions, in *Proceedings of Mathematics and Computation, Reactor Physics and Environmental Analysis in Nuclear Applications, Madrid Spain, September 27–30, 1999*, (Senda Editorial, S. A. Madrid Spain, 1999), Vol. 2, p. 1762 in book proceedings and p. 1912 in CD-ROM proceedings.
19. J. F. Briesmeister, Ed., *MCNP—A General Monte Carlo N-Particle Transport Code*, Version 4B, LA-12625-M (Los Alamos National Laboratory, NM, 1997).
20. J. Spanier and E. M. Gelbard, *Monte Carlo Principles and Neutron Transport Problems* (Addison-Wesley, Reading, MA, 1969).
21. T. Ueki, J. E. Hoogenboom, and J. L. Kloosterman, Monte Carlo forward-adjoint coupling by next event estimation, in *Proceedings of Mathematics and Computation, Reactor Physics and Environmental Analysis in Nuclear Applications, Madrid Spain, September 27–30, 1999*, (Senda Editorial, S. A. Madrid Spain, 1999), Vol. 1 p. 241 in both book and CD-ROM.